TRIBO-ELECTROANALYTICAL EVALUATION OF CMP SLURRIES AND POST-CMP CLEANING SOLUTIONS

David Santefort, Kassapa Gamagedara, and Dipankar Roy*
Clarkson University Physics Dept and CAMP, droy@clarkson.edu

INTRODUCTION

The tasks of advancing the processing chemistries for CMP and post-CMP cleaning (PCMPC) can be considerably aided in a time- and cost-effective approach by using tactically designed electrochemical tests with laboratory-level model systems. To maximize the benefits of such measurements, it is further necessary to simultaneously probe the (electro)chemical and tribological components of the processing mechanisms. Explorations of such "tribo-echem" testing protocols have been previously reported for certain metal CMP systems with a primary focus on open circuit potentials (OCP) and potentiodynamic polarization measurements [1-4]. In an effort to further expand these in situ methods of evaluating CMP chemistries, we have employed tribology coupled electrochemical impedance spectroscopy (EIS) along with tribo-OCP and tribo-polarization measurements, and additionally, quantified the framework of corresponding data analyses using the formalism of mixed-potential theory [5-9].

More recently, we have reported in situ tribo-echem studies of PCMPC model systems operated with brush-scrubbing of CMP-treated wafers [10, 11]. With illustrative new results, the current report presents a brief overview of some of these recent developments in the methodologies for evaluating CMP and PCMPC systems. Selected data sets are presented here from a collection of experiments involving different electrochemical techniques and different material-systems. Certain main capabilities of these measurement techniques are noted, both for qualitative and quantitative evaluations of processing variables in CMP/PCMPC. Instead of centering on a specific problem, the experimental results are collectively discussed as a brief synopsis of our group's recent studies in the area of CMP- and CMPC-chemistries.

EXPERIMENTAL

Fig. 1 schematically shows the tribo-electrochemical test cells used in this work to study model systems for (A) CMP and (B) PCMPC. In (A), the metal test sample for CMP (1″ diameter disc) served as a working electrode (WE) embedded in a Teflon holder [7]. The counter electrode (CE) was made of two stainless

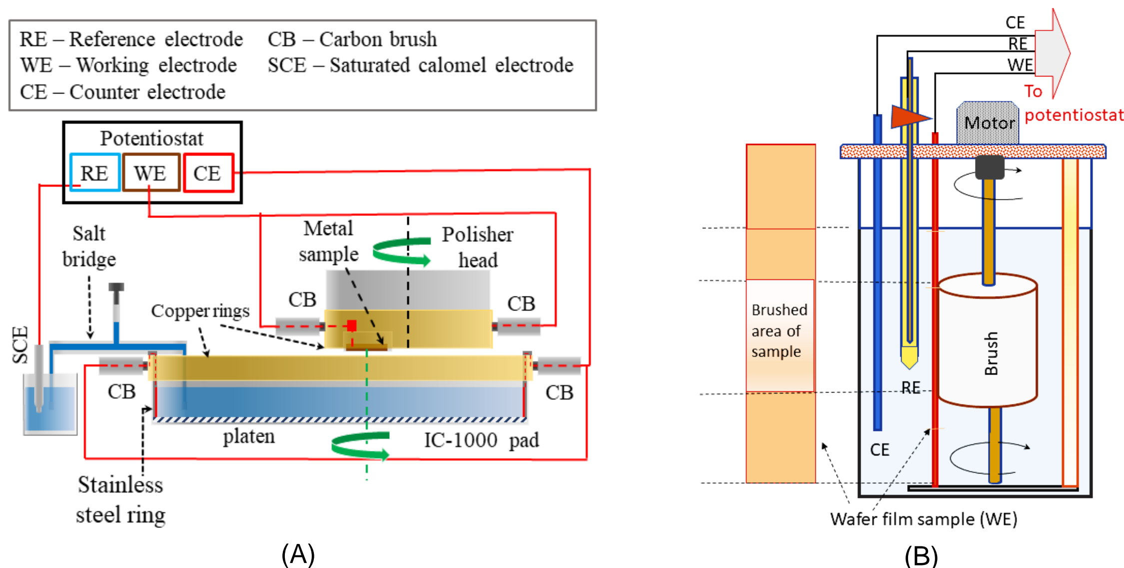

Fig. 1 Tribo-electrochemical test cell (A) integrated with a benchtop polisher for CMP, or (B) with a Poly(vinyl alcohol) (PVA) brush for PCMPC. Additional details are in the main text.

steel (SS) strips connected to a ring of SS placed along the cell's inner perimeter. The reference electrode (RE) was a saturated calomel electrode (SCE), used with a salt bridge (SB). Electrical connections (red lines) to the electrodes were enabled through carbon brushes (CB). The metal sample tested for CMP was polished at a 2 psi down-pressure on an IC 1000 pad with or without using colloidal silica abrasives. The electrochemically effective surface area of the metal sample was determined through measurements of the test cell's solution resistance as described previously [9].

In (B), a coupon cut out of a blanket wafer was used as a WE/test sample, positionally fixed in contact with a PVA brush with a brush-gap of -0.86 mm. The brush was turned at an angular speed of 60 rpm using a computer-controlled motor. A front-view of the PCMPC-WE sample is shown on the left side of the CE. The electrochemical signal generated at the brushed surface region of the WE was extracted by employing calculations based on Kirchhoff's rules [10]. The test cell used a RE of SCE and a SS strip as a CE.

Table 1. Comparison of CMP- and PCMPC-related corrosion parameters with and without the inclusion of the process-specific mechanical component[a]

Experimental system [Reference]	Consumables used to support surface chemistry	Measured variable for (metal sample)	Value without mechanical component	Value with mechanical component
CMP of Cu [7]	Slurry: 0.1 M MA + 50 mM SPC + 0.1 M $NaHCO_3$ (pH 9.3) + 5 wt% SiO_2	R_p (Cu) (kΩ cm^2)	1.28	0.61
		i_g (Cu-Co) (μA cm^{-2})	63.2	8.9
CMP of Co and Cu [8]	Slurry: 0.1 M KOAc + 0.3 wt% H_2O_2 + 1 mM BTA (pH 10.5) [a]	E_{corr}(Co) (V vs. SCE)	-0.31	0.18
		i_{corr} (Co) (μA cm^{-2})	20.9	43.2
CMP of Co and Cu [12]	0.1 M $NaHCO_3$ + 25 mM SPC + 1 mM BTA + 5 wt% SiO_2 (pH 10.3) 25 mM SPC + 0.5 wt%	i_g at Cu-Co contact (μA cm^{-2})	113	231
CMP of Ru and Ta [6]	Guanidine carbonate + 5 wt% SiO2.	i_{corr} (Ru) (μA cm^{-2}) i_{corr} (Ta) (μA cm^{-2})	83 3.5	229 3.7
PCMPC of Co and Cu [10]	Cleaner: 0.4 wt% oxalic acid at pH 11. CMP treatment: 0.1 M KOAc + 1 wt% H_2O_2 + 1 mM BTA at pH 10.5,	R_p (Co) (kΩ cm^2) R_p (Cu) (kΩ cm^2) i_{corr} (Co) (μA cm^{-2}) i_{cor} (Cu) (μA cm^{-2})	8.1 31.4 7.7 2.7	2.2 3.4 19.5 7.5
Post-CMP cleaning of Co and Cu [11]	Commercial post-CMP cleaning solution at pH 14	i_{corr} (Co) (μA cm^{-2}) i_{corr} (Cu) (μA cm^{-2})	2.2 2.0	60.0 111.0

[a] Process-specific mechanical component implies: Polishing of a metal disc sample on an IC 1000 pad for CMP, or scrubbing of a metal wafer sample with a PVA brush for CMPC. KOAc is potassium acetate (OAC ≡ $C_2H_3O_2$). SPC and BTA are sodium percarbonate ($Na_2CO_3 \cdot 1.5H_2O_2$, a solid-phase carrier of H_2O_2) and benzotriazole, respectively. MA (H_2Mal) denotes malonic acid (Mal ≡ $C_3H_2O_4$). The other terms/parameters in this Table are defined in the text.

DISCUSSION

The electrochemical parameters commonly used to evaluate CMP/PCMPC surface chemistries of metals/alloys include: OCPs, corrosion potentials (E_{corr}), corrosion current densities (i_{corr}); galvanic current densities (i_g); and polarization resistances (R_p). E_{corr}, i_{corr} and R_p generally serve as indicators of the surface passivation functions of corrosion inhibitors and/or mechanically removable surface complex films. R_p values also provide a convenient measure of the residual removal efficiencies of PCMPC chemistries [10]. In addition, i_{corr} is often utilized as an overall predictor of material removal capabilities of CMP slurry

formulations [1, 3]. While these variables are typically measured without the mechanical processing components (polishing for CMP and scrubbing for P-CMPC), several experiments have demonstrated how critically the measured values of such corrosion parameters are dictated by these mechanical actions. Table 1 presents a self-explanatory summary of some published results establishing this point.

Measurement of OCP transients in alternated cycles of polish (P) and stationary hold (H) at the CMP interface provide a traditional way of including tribology in electrochemical studies of CMP systems. This relatively straightforward method does not involve the complexities of area normalization to account for electrochemically active surface sites. Fig. 2A shows a typical example of such OCP transients recorded in the context of studying W-CMP, where (electro)chemical formation and mechanical removal of W-oxide surface films (predominantly WO_3 in this case) were examined in a preliminary trial solution of KNO_3-H_2O_2 before including other slurry-additives. The time scales of P and H sequences in these measurements were significantly extended beyond those of actual CMP process to examine the long-term electrochemical stability of the CMP interface.

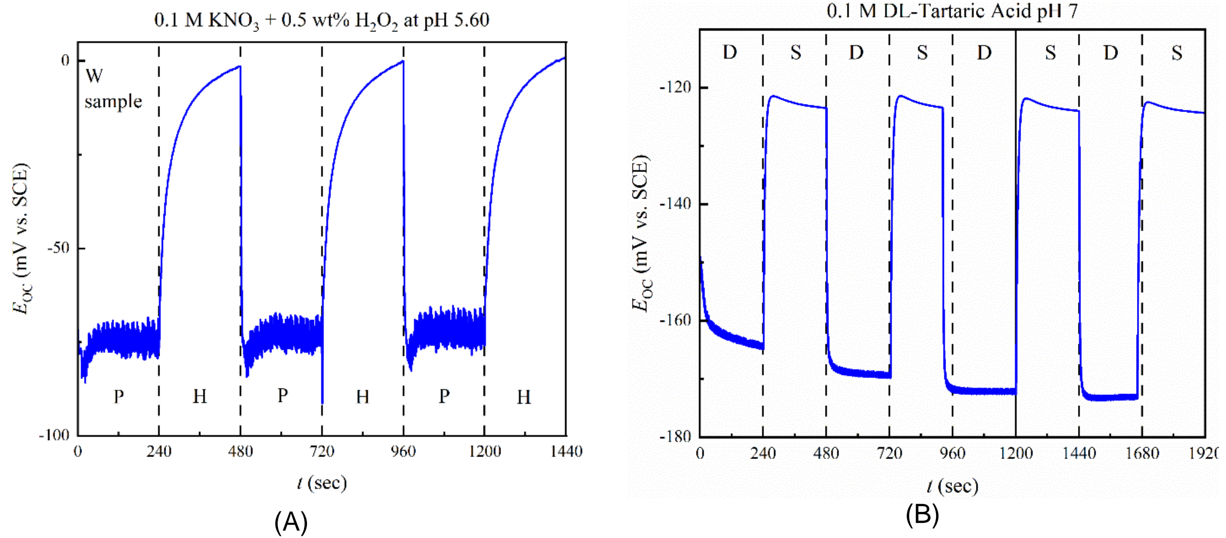

Fig. 2 Experimental data illustrating OCP (E_{oc}) transients recorded by including or excluding the mechanical components of (A) surface polishing with a pad for CMP of W, and (B) surface scrubbing with a PVA brush for PCMPC of Cu. Experimental systems: (A) A partially formulated slurry solution for W using 0.10 M KNO_3 + 0.5 wt% H_2O_2 at pH 5.6, and (B) an exploratory PCMPC solution for Cu employing 0.1 M DL tartaric acid at pH 7. The polish (P) and stationary hold (H) cycles for CMP as well as the dynamic (D) and static (S) brush operations for PCMPC were alternated in 4 min intervals.

The OCP measured in Fig. 2A is an equilibrium potential where the mixed potential reaction of surface film formation [$W + 3H_2O_2 = WO_3 + 3H_2O$] occurs due to a coupling between anodic oxidation [$W + 3H_2O = WO_3 + 6H^+ + 6e^-$] of W and cathodic reduction of hydrogen peroxide [$3H_2O_2 + 6e^- + 6H^+ = 6H_2O$]. The oxide film grows during each H stage in Fig. 2A, where the OCP increases due to increased anodic passivity of the test surface. The oxide film is structurally weakened by partial dissolution to WO_4^- and is removed in the next P sequence as indicated by a corresponding drop in the OCP value. These results are comparable to those previously reported for a similar W-CMP slurry at lower pH values [1].

The OCP response of an electrochemical interface to the latter's relative strengths of anodic and cathodic activities can be described using Eq. (1) below,

$$OCP \equiv E_{corr} \approx a + [b\ln(i_c^0 s_c / i_a^0 s_a)] \tag{1}$$

which is based on the mixed potential theory for a binary reaction system as the one considered for Fig. 2A, and accounts for the theoretical equivalence between OCP and E_{corr} [6]. Both a and b in Eq. (1) are defined in terms of the Nernst potentials and transfer coefficients of the mixed reaction's faradaic steps. i_c^0 and i_a^0 are the cathodic and anodic exchange current densities, respectively. s_c and s_a are the metal

sample's surface fractions supporting the cathodic and anodic steps of the mixed reaction, respectively. Conventional treatments of Nernst potentials in the CMP literature generally assume unit activity coefficients for all solid surfaces containing adsorbates. In this description, a and b, as well as the exchange current densities are defined by bulk concentrations of the reactants and products [13].

As long as the CMP slurry's chemical concentration at the pad-sample interface is not mass transfer limited and can be taken as a bulk concentration, the OCP under CMP conditions is predominantly determined by the values of s_c and s_a in Eq. (1). This assumption of bulk concentration can be verified by determining an electrical equivalent circuit (EEC) of the test system through complex nonlinear least square analyses (CNLS) of EIS data, and ensuring that the resulting EEC is free of diffusion elements. The currently available literature suggests that typical metal CMP systems are mostly in this diffusion-free category, and that the ratio (s_c/s_a) plays a leading role in dictating OCP values. The anodic activity (value of s_a) at a CMP surface decreases in the presence of surface passivating oxides, complexes and/or corrosion inhibitors. Thus, when the surface conditions (such as those of a stationary H stage) favor the growth of passive films, the OCP continues to rise until the surface coverages of these films reach saturation. The OCP drops again as the films are removed by abrasion in a P stage. The data in Fig. 2A follow this description of Eq. (1).

Using the example of Fig. 2, the following *analytical utilities* of polish-hold OCP transient measurements can be noted from simple visual inspections of the most prominent data-features. (1) *CMP-enabling surface film forming function of the slurry* is confirmed if a sizable gap exists between the OCP (H) and OCP (P) values. An OCP-increase in the anodic direction resulting from termination of polishing, as seen in Fig. 2A, usually confirms that the CMP chemistry supports anodically passivating surface films. (2) *Effective removal of these films by polishing* is evidenced in a fully reversed (cathodic) OCP shift in a subsequent polish cycle. (3) *Steady state operation of CMP* requires that the rate of surface film removal via abrasion be matched by the rate of film formation via (electro)chemical reactions. Time independent OCP plots as those collected during the P cycles in Fig. 2A indicate steady state occurrence of CMP. (4) *Electrochemical stability and repeatability of slurry functions* are indicated in the existence of closely comparable OCP profiles generated by recurrently operated H and P cycles as those found in Fig. 2A. More in-depth analyses of surface chemistries, such as probing the kinetics of surface film formation and removal can be carried out by fitting polish vs. hold OCP data to an appropriate kinetic model in the formulation of Eq. (1) [7].

To check the chemical and mechanical functions of PCMPC within a single data set, OCP transients can be recorded using a setup like that of Fig. 1B, and operating the scrubbing brush in alternated dynamic (rotated while pressing onto a wafer sample) and static (stationary while pressing onto the sample) cycles. To collect the illustrative results shown in Fig. 2B, a Cu wafer sample was pretreated in a CMP solution of 0.01 M glycine (HGly as zwitterion, Gly = $C_2H_4NO_2$) + 1 mM BTA + 0.1 wt% H_2O_2 at pH 6. The main residues of CMP on the Cu wafer surface in Fig. 2B include Cu_2O, CuO, CuBTA and $CuGly_2$ [2]. In the PCMPC solution, DL-tartaric acid, H_2T (T = $C_4H_4O_6$) removes Cu_2O and CuO in the forms of CuT_2^{2-} and $CuT_2(OH)_2^{4}$, respectively.

The OCP in Fig. 2B represents a mixed reaction between the cathodic reduction of O_2 and anodic dissolution of Cu_2O as CuT_2^{2-}. Some of the CuT_2^{2-} and $CuT_2(OH)_2^{4-}$ species remain embedded in the Cu surface film during the recording of the S-segments of OCP collection. Under this condition, the surface is anodically less active, i.e., the area-ratio, (s_c/s_a), and hence the OCP is at its higher value. Dynamic brushing removes the anodic suppressor adsorbates, thereby decreasing the value of (s_c/s_a) and consequently, that of E_{oc}. Residue removal quickly reaches a saturation level of surface cleaning, which is indicated in the time independent OCP (D) data. The largely time independent OCP (S) data indicate fast re-adsorption of CuT_2^{2-} and $CuT_2(OH)_2^{4-}$ onto the cleaned surface upon termination of dynamic brushing.

The experimental approach in Fig. 2B is similar to that of P-H transients considered for CMP in Fig. 2A; the overall results for the two cases also appear mutually similar. However, the volume of the "residues" removed from the PCMPC surface in Fig. 2B is significantly smaller than that of the fully formed "surface films" removed from the CMP surface in Fig. 2A. This difference contributes to the noticeable reduction in the gap seen between OCP(D) and OCP (S) in Fig. 2B compared to that recorded between OCP (P) and OCP (H) in Fig. 2A. Nevertheless, the faradaic activities of the removed species as well as the sample

substrates are material-specific for the two different systems. These factors also contribute to the different ranges of OCP variations observed between Fig. 2A for W and Fig 2B for Cu.

Potentiodynamic polarization measurements are necessary to determine corrosion parameters for CMP and PCMPC systems. These experiments also help to examine the individual variations of s_c and s_a in Eq. (1). The latter test is necessary for quantitative data analyses because, as noted in the context of Fig. 2, the response of OCP transients to mechanical and/or chemical perturbations is only manifested as an overall change in the *ratio* (s_c/s_a). Fig. 3 shows an exemplary set of tribology-controlled (A) polarization

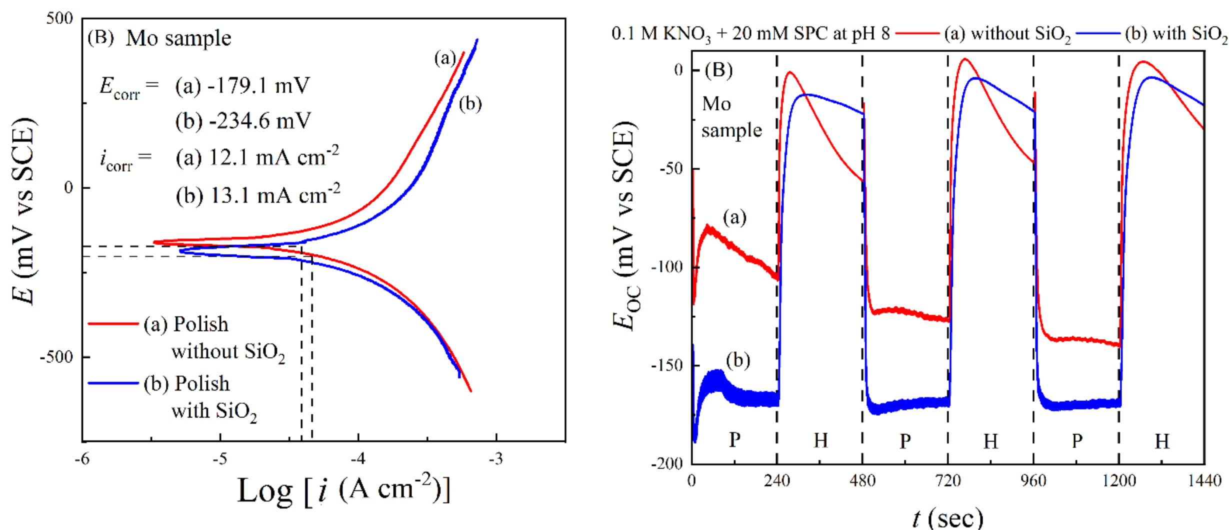

Fig. 3 (A) Potentiodynamic plots (a) and (b) recorded under surface polishing of a Mo sample at a voltage scan rate of 5 mV s^{-1} without (a) or with (b) including 5 wt% colloidal SiO_2 in a moderately alkaline test slurry for Mo-CMP. (B) Lines (a) and (b) represent OCP (E_{oc}) transients recorded in alternated stages of polishing (P) and stationary hold (H) under the same conditions of plots (a) and (b) in Fig. 3A, respectively. The slurry composition is common for (A) and (B), and is indicated above panel (B).

data for a CMP system of molybdenum, along with (B) polish-hold OCP transients recorded for this system. In these experiments, H_2O_2 from SPC in the slurry is cathodically reduced [H_2O_2 + 2e- = $2OH^-$] and Mo is anodically oxidized [Mo + $6OH^-$ = MoO_3 + $3H_2O$ + 6e-] which result in the net reaction, Mo + $3H_2O_2$ = MoO_3 + $3H_2O$. This coupled reaction leads to the mixed potential, recorded as E_{oc} in Fig. 3B. The unstable MoO_3 film becomes porous due to dissolution [MoO_3 + $2OH^-$ = MoO_4^{2-} + H_2O], as seen in the decaying OCP during H stages. The remaining film is removed by polishing at a low pressure (2 psi used in this study).

The polarization (Tafel) plots in Fig. 3A have been normalized with respect to the electrochemically effective area of the Mo sample surface [12]. Both plots (a) and (b) represent the aforesaid mixed potential reaction of MoO_3 surface film formation and polishing removes this film as it forms. The upper and lower current branches of each Tafel plot represent the anodic oxidation of Mo and cathodic reduction of H_2O_2, respectively. The E_{corr} values found from the Tafel plots are noted in Fig. 3A. The corrosion current densities (i_{corr}) were determined by Tafel extrapolations, and as indicated in the figure, polish-assisted i_{corr} increases when abrasive particles are used. This shows an active role of silica in the removal of MoO_3 from the Mo surface. The material removal rate (MRR) gravimetrically measured for the *polycrystalline Mo disc* sample was ~30 nm min^{-1}. The mechanism of material removal in this case is linked to chemically and mechanically controlled tribo-corrosion of Mo in the CMP environment.

In Fig. 3B, E_{oc} increases during the H stage indicating a corresponding increase in the ratio, (s_c/s_a), which occurs by decreasing s_a, owing to a growth in the anode-blocking Mo-oxide surface film. This effect is reversed in the P stage. The P vs H features are largely repeated with recurrent cycles, indicating slurry stability. Due to different measurement conditions of E_{oc} and E_{corr}, the E_{oc} (P) values are somewhat different from their E_{corr} counterparts in Fig. 3A, and this is consistent with previous observations [7, 8]. The E_{oc} (P) monitored with SiO_2 in Fig. 3B is consistently lower than E_{oc} (P) without SiO_2; the E_{corr} in Fig. 3A also

displays the same trend. In the description of Eq. (1), this suggests that that the value of (s_c/s_a) established during abrasive assisted polishing is lower than that supported during abrasive free polishing. This effect can be attributed to a relatively higher efficiency of oxide removal (increased s_a) for the silica-added slurry.

The dataset of E_{oc} alone is not sufficient to fully confirm the foregoing explanation, because OCP transients only reflect variations in the (s_c/s_a) *ratio* but do not indicate how selective changes of the *individual* terms, s_c and s_a (preferential changes in the sample's anodic or cathodic activity) govern the resulting ratio of [*cathodic vs. anodic*] site coverages. A clarification of this latter point comes from the potentiodynamic data shown in Fig. 3A. In the transition from SiO_2-free to SiO_2-added slurries, the anodic (upper) branch of (b) shifts toward higher currents compare to the corresponding currents for (a); this clearly shows that the anodic activity (value of s_a) of the Mo surface preferentially increases in the case of SiO_2 assisted polishing. This increase in s_a (rather than a decrease in s_c) is responsible for causing a net decrease in the value of (s_c/s_a), which in turn leads to the cathodic shift of E_{oc} (P) in the presence of abrasives.

EIS measurements use a broad range AC perturbation spectrum of average amplitude E (5-10 mV) applied to the experimental interface. The resulting current's magnitude (i) and phase (ϕ) are measured as functions of the perturbation frequency (f, or $\omega = 2\pi f$). The real (Z') and imaginary ($-Z''$) parts of the complex impedance (Z) are obtained as: $Z' = |Z| \cos\phi$ and $Z'' = |Z| \sin\phi$, with $|Z| = |E|/|i|$. EIS results are plotted as [$Z'(\omega)$ vs. $-Z''(\omega)$] (Nyquist impedance), or [$|Z|$ (f) vs. log f] (magnitude Bode), or [ϕ (f) vs. log f] (phase Bode). Practical utilization of EIS is subject to four data-validation criteria (stability, linearity, causality and finiteness). For transient CMP-related systems, establishing experimental conditions to meet these criteria often becomes difficult, and may be unachievable in some cases [14].

An experimental approach to EIS validation has been illustrated previously [14]. In this approach, the stability test is performed first by superimposing data from several sets of consecutive measurements to check if the different data-sets overlap showing their temporal stability. If this test confirms system-stability over an adequate frequency range to perform CNLS analysis of the data, several subsequent tests for EIS validation are performed. Linearity of the data can be validated by repeating the measurements with AC perturbation voltages of at least two sufficiently different values in the 5-10 mV range, and by ensuring that these different perturbations yield the same impedance spectrum. A check for causality requires a rigorous process of input-output frequency comparison. The finiteness criterion of EIS can be warranted if the CNLS-analyzed EEC of the test interface yields finite impedances in the limits $f \rightarrow 0$ and $f \rightarrow \infty$.

Three trials of Nyquist impedance plots successively recorded for a Cu CMP sample during polishing using the test cell in Fig. 1A are superimposed in Fig. 4A. The slurry solution and the other relevant parameters are indicated in the figure. The data for the three plots are largely overlaid onto each other and thus, they meet the temporal stability requirement of EIS validation. CNLS analyses of these data yield a previously discussed EEC [7], which is in compliance with the requirement of finite impedance and contain the essential resistive elements, R_s (solution resistance) and R_p (polarization resistance) [9]. Fig. 4B shows an example of a system for Cu-PCMPC where the low-frequency (right-most) regions of three consecutively collected Nyquist plots do not overlap and hence do not meet the stability criterion of EIS. This system was not subjected to additional validation tests, and was identified as unsuitable for probing by EIS.

EIS can be used to estimate the residue removal efficiency (RRE) of PCMPC formulations ($0 \leq$ RRE ≤ 1). This application requires the following three differently pretreated coupon samples of a test wafer: (i) a CMP-treated sample fully exposed to the CMP process that would generate post-CMP residues; (ii) a CMP+PCMPC-treated sample that is CMP processed as sample (i) and then cleaned with the test solution of PCMPC, and (iii) a PCMPC-only sample that has not been subjected to CMP, but has been exposed to PCMPC using the same solution and procedure used to clean sample (ii). The three samples are then examined with EIS at the OCP in a pH-neutral, non-reactive sensing solution like that of KNO_3 or sodium phosphate at a moderate (0.05-0.1 M) concentration. The polarization resistance of the sensing interface is determined for each sample by CNLS-fitting EIS data individually recorded for the three samples.

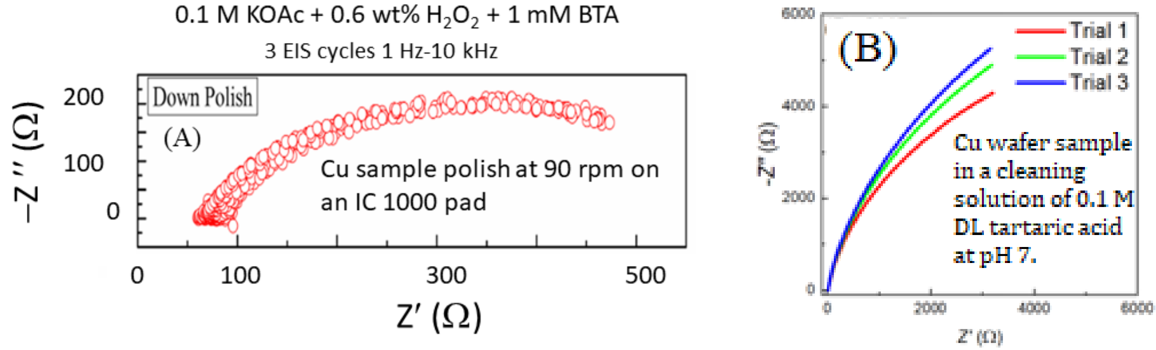

Fig. 4. (A) Successively recorded and superimposed Nyquist impedance data for a Cu CMP sample demonstrating implementation of the stability criterion of EIS. (B) An example of temporally unstable EIS data set recorded for a Cu PCMPC interface.

A working formula for EIS-based RRE measurements can be derived with the following assumptions: (A) CMP residues block surface sites available for faradaic charge transfer at the cleaning interface and thereby increases R_p of the test samples; and (B) The PCMPC-only sample (iii) described above is the cleanest one in the experimental group while site-blocking by residues is most prevalent for sample (i). Based on these assumptions, we define: RRE = $[1-(\theta_{rc}/\theta_{r0})]/[1-\theta_{rc}]$, where θ_{r0} and θ_{rc} are fractional coverages of CMP residues residing on the sample surface, respectively, before and after the sample's PCMPC ($\theta_{rc} < \theta_{r0}$). Using the assumptions mentioned above, the RRE can be formulated in terms of the polarization resistances, R_p (CMP), R_p (CMP+PCMPC) and R_p (PCMPC), measured in the sensing solution for samples (i), (ii) and (iii), respectively:

$$\mathrm{RRE} = \frac{1-(\theta_{rc}/\theta_{r0})}{1-\theta_{rc}} \equiv \frac{[1/(1-\theta_{r0})]-[1/(1-\theta_{rc})]}{[1/(1-\theta_{rc})]-1} = \frac{R_p(\mathrm{CMP})\text{-}R_p(\mathrm{CMP{+}PCMPC})}{R_p(\mathrm{CMP})\text{-}R_p(\mathrm{PCMPC})} \qquad (2)$$

where it is also assumed that R_p is inversely proportional to the fractional surface area available for interfacial charge transfer, which has the values, $(1-\theta_{r0})$, and $(1-\theta_{rc})$, before and after cleaning the residues, respectively. For the PCMPC-only sample ii) we take $\theta_r \approx 0$. Analytical validity of this RRE formula is embedded in the latter's limiting values: RRE $\rightarrow 0$ when $\theta_{rc} = \theta_{r0}$, and RRE $\rightarrow 1$ when $\theta_{rc} = 0$.

Fig. 5A-F displays demonstrative results of EIS in the form of Bode plots, recorded for a Cu wafer sample in a sodium phosphate sensing solution, to measure the RRE of a PCMPC method that used a malonic acid based cleaner. The CMP pretreatment and the CMP residues on the Cu surface are the same as those mentioned in Fig. 2B. The main cleaning chemistry considered here is the removal of CuO by dissolution [$CuO + 2Mal^{2-} + H_2O = CuMal_2^{2-} + 2OH^-$], as well as secondary removal of CuBTA and Gly co-adsorbed with CuO. Mutually superimposed data sets in panels A-F demonstrate EIS-stability. Fig. 4G shows R_p values determined from the EIS data, along with the RREs obtained by using these R_p data in Eq, (2).

CONCLUSIONS

Tribo-electrochemical tests using bench-top model systems can play a significant supporting role in the optimization of surface chemistries that are needed to promote defect-free, efficient performances of CMP and PCMPC processes. Although this approach (based on typical lab-settings) does not allow one to fully mimic the actual material-layouts or the manufacturing conditions of device fabrication, such experiments can provide a wealth of useful material-specific information about the essential CMP/PCMPC characteristics of an exploratory system. Adding previously unpublished new results to our recently reported findings in this area, we have demonstrated further in this work how the capabilities of electro-analysis for evaluating CMP/PCMPC systems can be enhanced by combining electrochemical measurements with the tribology-controlled essential features of CMP and PCMPC.

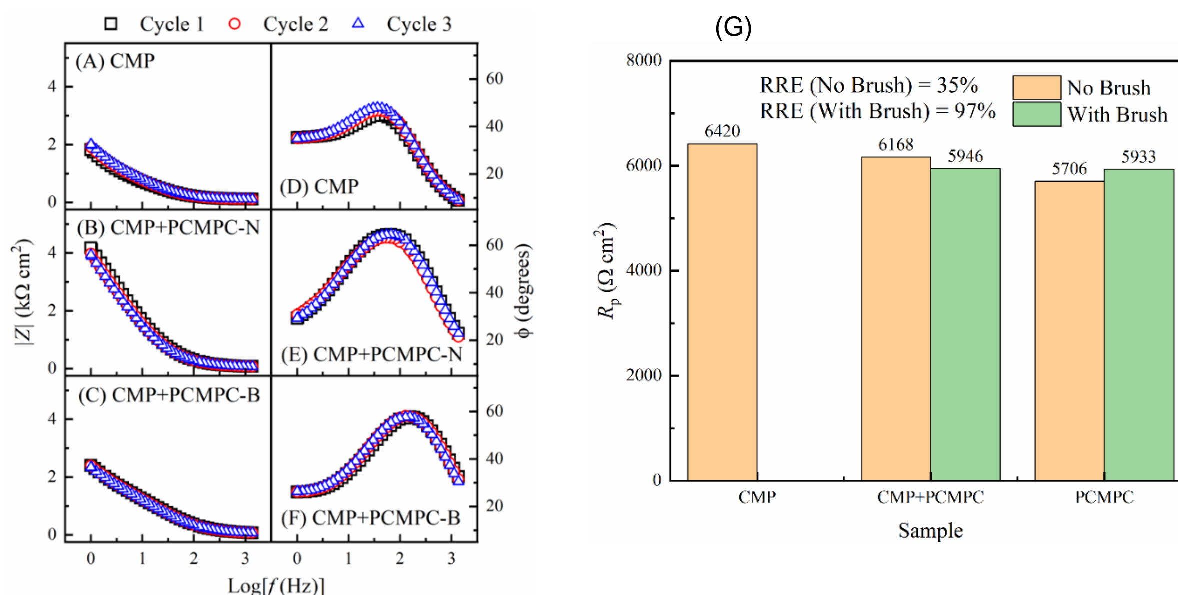

Fig. 5. (A-F): Amplitude (□) and phase (○) Bode plots from three consecutive cycles of area normalized EIS obtained in a pH-neutral sensing solution of sodium phosphate using CMP-treated Cu samples that underwent different types of subsequent PCMPC treatments. "-B" and "-N" denote surface cleaning with or without brush-scrubbing, respectively. (G): Values of R_p obtained by analyzing the EIS data.

ACKNOWLEDGEMENTS

The authors thank Drs. Michael White and Jun Liu of Entegris, Inc. for supporting the construction of the PCMPC brush cell and for providing the wafer samples and Planarcore PVA brushes used with the cell.

REFERENCES

[1] E Kneer, C Raghunath, V Mathew, S Raghavan, JS Jeon. J. Electrochem. Soc. 1997;144:3041.
[2] S Aksu, FM Doyle. J. Electrochem. Soc. 2002;149:G352.
[3] DJ Stein, D Hetherington, T Guilinger, JL Cecchi. J. Electrochem. Soc. 1998;145:3190.
[4] S Shima, A Fukunaga, M Tsujimura. ECS Trans. 2007;11:285.
[5] D Roy. ECS J. Solid State Sci. Techn. 2018;7:P209.
[6] X Shi, DE Simpson, D Roy. ECS J. Solid State Sci. Techn. 2015;4:P5058.
[7] S Wei, C Johnson, D Roy. ECS J. Solid State Sci. Tech. 2021;10:034001.
[8] C Johnson, S Wei, D Roy. ECS J. Solid State Sc.Techn. 2018;7:P38.
[9] M Turk, M Walters, D Roy. Mater. Chem. Phys. 2017;201:271.
[10] C Johnson, D Roy. ECS J. Solid State Sci. Techn. 2019;8:P3163.
[11] C Johnson, J Liu, M White, D Roy. ECS J. Solid State Sci. Techn. 2021;10:054005.
[12] MC Turk, X Shi, DAJ Gonyer, D Roy. ECS J. Solid State Sci. Techn. 2016;5:P88.
[13] D Gray, A Cahill. J. Electrochem. Soc.. 1969;116:443.
[14] MC Turk, MJ Walters, D Roy. Electrochim. Acta. 2017;224:355.

* Corresponding Author:
Dipankar Roy
Tel: +1 315-268-6676
E-mail: droy@clarkson.edu
Clarkson Physics, P.O. Box 5820
Potsdam, NY 13699-5820, USA

Presentation Preference:

■ Oral ☐ Poster

Topic Area:
Defects and Post CMP cleaning